



An Experimental Study of Microstructure-Property Relationships in Thermal Barrier Coatings

M. Gupta, G. Dwivedi, P. Nylén, A. Vackel, and S. Sampath

(Submitted October 16, 2012; in revised form February 10, 2013)

The thermal-mechanical properties of thermal barrier coatings are highly influenced by the defects present in coating microstructure. The aim of this study was to meet the future needs of the gas turbine industry by further development of zirconia coatings through the assessment of microstructure-property relationships. A design of experiments was conducted for this purpose with current, spray distance, and powder feed rate as the varied parameters. Microstructure was assessed with SEM and image analysis was used to characterize porosity content. Evaluations were carried out using laser flash technique to measure thermal properties. A bi-layer beam curvature technique in conjunction with controlled thermal cycling was used to assess the mechanical properties, in particular their nonlinear elastic response. Coating lifetime was evaluated by thermo-cyclic fatigue testing. Relationships between microstructure and coating properties are discussed. Dense vertically cracked microstructure and highly porous microstructure with large globular pores were also fabricated. Correlations between parameters obtained from nonlinear measurements and lifetime based on a priori established microstructural analysis were attempted in an effort to develop and identify a simplified strategy to assess coating durability following sustained long-term exposure to high temperature thermal cycling.

Keywords design, lifetime, microstructure, nonlinear degree, thermal barrier coatings, thermal conductivity, Young's modulus

1. Introduction

Atmospheric plasma-sprayed (APS) ceramic coatings are commonly used for thermal protection of components as thermal barrier coatings (TBCs) in gas turbine engine applications (Ref 1). Application of TBCs can provide increased engine performance/thrust by allowing higher gas temperatures or reduced cooling air flow, and/or increased lifetime of turbine blades by decreasing metal substrate temperatures. Increase in both efficiency and specific power is in high demand for both aero turbines and industrial gas turbines for their further development. This demand implies the requirement that the thermal conductivity of the ceramic coating should be minimized and also that the value should remain low during prolonged exposure to service conditions.

M. Gupta and P. Nylén, University West, 461 86 Trollhättan, Sweden; G. Dwivedi and A. Vackel, Center for Thermal Spray Research, Stony Brook University, Stony Brook, New York 11794; and S. Sampath, University West, 461 86 Trollhättan, Sweden and Center for Thermal Spray Research, Stony Brook University, Stony Brook, New York 11794. Contact e-mail: mohit-kumar.gupta@hv.se.

TBC is a duplex material system which consists of an intermediate metallic bondcoat and an insulating ceramic topcoat. Most commonly used ceramic material for topcoats is yttria-stabilized zirconia (YSZ) due to its favorable thermal and mechanical properties. Topcoat microstructures in TBC applications are highly heterogeneous, consisting of defects such as pores and cracks of different sizes. Evolution of the complex microstructure of YSZ coatings is highly sensitive to processing conditions and feedstock (Ref 2-8). The morphology of this complex microstructure determines the coating's final thermal and mechanical properties, and the service lives of the coatings (Ref 9-13). Thus, understanding of process microstructure-property relationships is of prime scientific and technological interest.

Recent studies have shown that ceramic coatings exhibit anelastic mechanical response (Ref 14-17). Their behavior particularly under tensile loading is strongly nonlinear. In general, increasing tensile stress results in a lower value of coating modulus (Ref 14, 18-20). The nonlinearity is driven by unique microstructural features present in the TBCs, specifically micro-cracks and weak splat interfaces. The opening and closing of cracks and sliding of sprayed lamellae over each other give rise to a nonlinear response. The apparent stiffness decreases with increasing tensile stress as the cracks faces open apart, while it increases with increasing compressive stress as the cracks faces are closed together. All of the above measurements were obtained from bi-layer beam curvature measurements with controlled low temperature thermal cycling. This technique here-in referred to as the ex situ coating property sensor (ECP) sensor an attractive tool

for evaluating the mechanical properties of TBCs as it has been shown capable of capturing their nonlinear mechanical response (Ref 15-17).

The objective of this work was to achieve a topcoat microstructure exhibiting high performance, that is providing high insulation and having long lifetime. Fundamental relationships between microstructural features, thermal-mechanical properties of TBCs and their lifetime are discussed. Note that this study was limited to the changes in lifetime only due to changes in topcoat microstructure. The effect of changing bondcoat material on mechanical properties and lifetime of TBCs was not considered in this work.

2. Experimental Procedure

2.1 Sample Production

All coatings investigated in this study were deposited with atmospheric plasma spraying. Sulzer Metco F4 gun was used for this purpose. The topcoat material used in this study was agglomerated and sintered 7 wt.% YSZ (Starck Amperit 827). The bondcoat material used was NiCoCrAlY (AMDRY 365-2). The spray conditions for bondcoat were the same for all the samples. The thickness of sprayed topcoats was approximately 500 μm and bondcoats was approximately 200 μm . The substrates were made of the nickel based superalloy Hastelloy-X. All substrates were grit-blasted with Al_2O_3 -60 mesh before spraying.

A preliminary investigation was conducted to analyse the effect of substrate temperature on the sprayed topcoat microstructure. It has been observed earlier that higher substrate temperature during coating deposition leads to reduced porosity due to improved inter-splat contact (Ref 21). However, it must be noted that these results would highly depend on the powder morphology and the testing conditions. Specialized fixture was developed to conduct tests for this study. The rotating fixture has possibility for both in situ electrical heating and water cooling, so as to maintain the specified temperature during the spray trials. Three sets of ten samples can be sprayed at the same time with different substrate temperature for each set. The temperature is measured on the back side of the substrate with a thermocouple. External air cooling is also used when the samples are being sprayed. With this set-up, the substrate temperature can be maintained within ± 5 $^\circ\text{C}$ of the specified value. The set-up is shown in Fig. 1. It must be noted here that measured substrate temperature would be lower than the actual substrate temperature due to the presence of a temperature gradient across the substrate thickness. Topcoat material used for this study was high purity agglomerated and sintered YSZ (Sulzer Metco). Cylindrical coupons with dimensions $\Phi 25.4 \times 6.5$ mm were used as substrates. Substrate temperatures used were no external heating/cooling, 250, 350, 450, and 550 $^\circ\text{C}$. Substrate temperatures higher than 550 $^\circ\text{C}$ were not considered in this study due to the infeasibility with upscaling the process on large components.

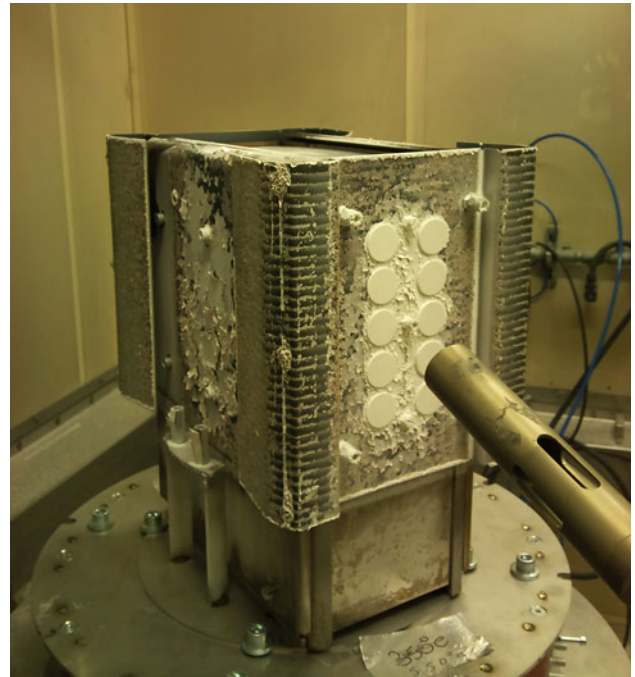


Fig. 1 The experimental set-up for substrate temperature sensitivity tests

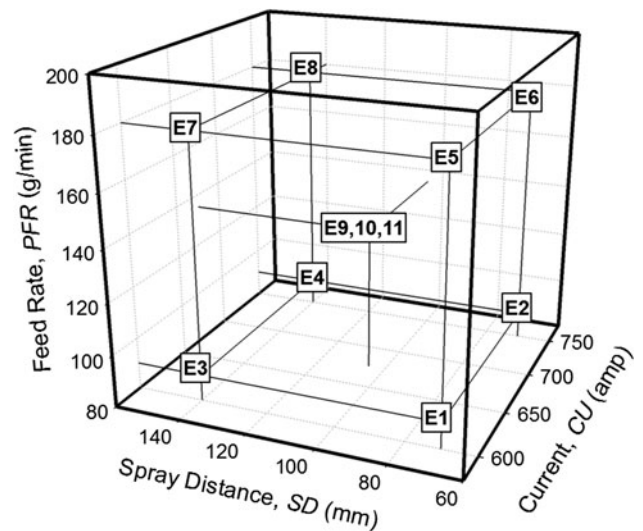
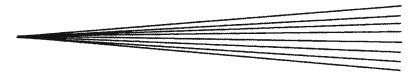


Fig. 2 The experiment design showing the spray settings (E1, E2,... represent the experiment number)

A design of experiments (DoE) was conducted for the main study in this work. A two-level full factorial design for three spray parameters was chosen, with 11 spray settings in total, as shown in Fig. 2. The experiments were

**Table 1 Spray parameters used for the spray trials**

Current	
Low	600 A
High	750 A
Spray distance (feed rate)	
Low	70 mm (4.5 mm/rev)
High	140 mm (6.5 mm/rev)
Powder feed rate (per injector)	
Low	45 g/min
High	90 g/min
Primary gas (Argon) flow	38 NLPM
Secondary gas (Hydrogen) flow	12 NLPM
Surface velocity	80 m/min

performed in a randomized run order so as to avoid the effect of external parameters, such as air temperature, humidity, etc.

As described later in section 3.1, it was seen that increasing the substrate temperature could not produce a statistically significant difference in porosity in topcoat microstructure. So it was not selected as one of the varied spray parameters for the design matrix.

Current (CU), spray distance (SD), and powder feed rate (PFR) were considered to be the most influential in achieving a varied topcoat microstructure, and so they were used in the design matrix. The high and low values of these three parameters along with the other spray parameters used are shown in Table 1. Two injectors were used to feed the powder into the plasma for high powder feed rate. The samples were mounted on a rotating carousel and a robot arm was used to move the spray gun in the vertical direction. When the spray distance is short, the plasma plume becomes too narrow where the molten particles impact the substrate. Due to a large variation in spray distance, the robot vertical speed feed rate had to be changed along with the spray distance otherwise threads of sprayed material were formed on the substrate. However it should be noted that the robot vertical speed was changed only when spray distance was changed and not varied independently.

Substrates with dimensions $30 \times 30 \times 1.54$ mm were sprayed for microstructure and thermal conductivity analysis. Substrates for thermo-cyclic fatigue tests were in dimensions $50 \times 30 \times 5$ mm.

2.2 Microstructure and Image Analysis

A sample from each set of coatings was sectioned using a diamond cutting blade, and then mounted and polished in cross section using a standard procedure for TBCs. Samples were then inspected using optical microscopy and scanning electron microscopy (SEM).

The porosity measurement was carried out using an image analysis routine developed earlier (Ref 22). According to this procedure, 20 images were taken across the coating cross section to represent the coating microstructure. The images were then processed using the Aphelion (version 3.2) image analysis software (ADCIS, France).

During the image analysis procedure, the image (originally in gray scale) is converted into binary format by the use of thresholding, with the matrix represented by the black and the porosity by the white. This is normally operator dependent for which reason an auto-thresholding algorithm was used to avoid any errors caused by operator variations.

2.3 Thermal Conductivity

Thermal diffusivity was measured on the samples in this study using the widely accepted laser flash technique. A Netzsch Laser Flash Apparatus LFA 427 system (Netzsch Gerätebau GmbH, Germany) was used for measurements at room temperature (Ref 23).

10 mm disks were cut out from the sprayed samples using water jet cutting for thermal diffusivity tests. Thermal diffusivity of the whole TBC system was measured for each spray setting. Samples of substrate and substrate with sprayed bondcoat were analyzed for thermal diffusivity and specific heat capacity separately. Thermal diffusivity of topcoat was calculated afterwards from the measured values and the thicknesses of each layer. Thicknesses of each layer were measured from microstructural cross sections taken by an optical microscope.

A laser pulse is shot at the substrate face of the sample and the resulting temperature increase is measured with an InSb infrared detector. The signal is then normalized and thermal diffusivity is calculated using the following equation:

$$\lambda = (0.1388L^2)/t_{(0.5)}$$

where λ is thermal diffusivity, L is the thickness of the sample, and $t_{(0.5)}$ is the time taken for the substrate face of the sample to reach a half of its maximum rise. Each measurement is an average of five laser pulse shots spread out over 5 min. An average of two samples for each spray setting was considered to be the final value.

Samples were coated with a thin layer of graphite before the measurements. Since YSZ layer is translucent to light in the wavelength of the laser, the presence of graphite layer is essential to prevent the laser pulse from traveling through YSZ.

The density of topcoats was calculated from their respective porosity content and the density of a previously analyzed YSZ coating using the simple rule of mixtures. The porosity content was calculated using the same image analysis procedure as described earlier in section 2.2. This data was used to calculate the thermal conductivity of all samples. The specific heat capacity used for all coatings was 0.489 J/g·K. The density used was 5.566 g/cm³ with E11 coating as the reference porosity level for calculating densities of other coatings. The specific heat capacity and density values were used from previous data.

It has been observed earlier that sintering in plasma-sprayed TBCs can have a dramatic effect on coating microstructure and thermal properties (Ref 24-26). Samples for each spray setting were exposed to a short heat treatment to study the sintering resistance of the topcoats.

The samples were placed in a furnace at 1100 °C with normal atmosphere for 25 h and then analyzed for thermal conductivity in the same fashion as described earlier in this section.

2.4 Mechanical Testing

Bi-layer curvature measurement using specially developed continuous beam curvature monitoring during thermal cycling was used in this study to evaluate the mechanical behavior of the sprayed coatings. This technique allows for coating property estimation after deposition and hence termed *ex situ* coating property or ECP sensor. Deposits were made on grit-blasted Al 6061 substrates, 225 × 25 × 2.25 mm mounted on the *in situ* curvature measurement systems termed *in situ* coating property (ICP) sensor (Ref 27, 28). Non bondcoat was sprayed on these plates. The plates were grit-blasted on both sides to provide uniform stresses due to grit blasting. ICP sensor consists of noncontact displacement lasers and thermocouples to monitor the displacement and temperature, simultaneously, at the back of the sample during spraying and during the subsequent heat-cool cycle.

Aluminum was chosen as the substrate since it has relatively low stiffness which provides significant deflection and high thermal mismatch with YSZ which provides higher resolution for curvature-temperature measurements. Furthermore, the net thermal expansion mismatch between YSZ and Al between room temperature to the ECP cycling temperature of 250 °C is similar to that of a bondcoat sprayed superalloy-YSZ (three-layer system) combination when cycled between 1100 °C to ambient. The ECP measurements are done twice for each coating on aluminum substrate; the data for second thermal cycle is used for analysis. In comparison to a three-layer system, for the first two thermal cycles to a high temperature (1100 °C) without any significantly long isothermal exposure, the TGO growth will not be significant enough to impart any additional curvature change to the system. Therefore, the measurement conducted on Al-YSZ system should reflect similar results for topcoat as on a three-layer system, at least for the aforementioned thermal cycling conditions.

The specimens were then thermally cycled using ECP for *ex situ* curvature monitoring. In this version of ECP set-up, the specimen is heated inside a muffle furnace (Thermolyne-F6018) to provide a uniform heating and cooling with a through thickness temperature difference of 1-2 °C. For a heat cycle, the specimen is mounted vertically on the ECP sensor; it is then heated up to 250 °C and is cooled down back to the room temperature. Typically, this process takes 30 min for heating from room temperature to the maximum temperature, and approximately 10 h for cooling. In order to shorten the cooling time, the specimen is taken out of the furnace at around 180 °C to cool down in the ambient condition. A self-adhesive thermocouple (SA1XL-K-72, Omega Engineering Inc.) is glued on the substrate side of specimen for accurate measure of the temperature (Ref 17).

A detailed description of the coating's anelastic behavior is given in previous studies (Ref 15-17). These studies discuss the steps to calculate the nonlinear elastic relations from the low temperature thermal cycle data using a phenomenological constitutive uniaxial stress-strain (σ -) model. The model describes an asymmetric response under tension and compression with linear response under large compression as most of the cracks and thin defects will be closed. At a particular transitional stress value σ_T ($\neq 0$), the stress-strain relation changes from linear to nonlinear.

After processing the curvature-temperature data via an inverse analysis technique, required material parameters were estimated to describe the complete stress-strain relation of the coating. For the sake of consistency, the measurements in the temperature range of around 25-200 °C were used in all the specimens.

Two key parameters were identified from the inverse analysis: Young's modulus at room temperature (E), and nonlinear degree (ND). ND quantifies the nonlinear behavior of a coating and is described as

$$ND = E/E_{0.001}$$

where $E_{0.001}$ is the secant modulus between the transitional point ($\sigma = \sigma_T$) and stress-strain state at $\epsilon = 0.001$. A large ND value signifies greater nonlinearity while $ND = 1$ if a coating is linear elastic. Since each coating has its own unique stress-strain behavior resulting from its overall microstructures, these two parameters represent a quantitative measure of coating properties.

A major advantage of curvature measurement under temperature change is that it produces a more uniform stress state within a coating than that under mechanical load, as it does not generate stress concentration near load points.

2.5 Thermo-cyclic Fatigue

Thermo-cyclic fatigue (TCF) lifetime is one of the major criterions for assessing the performance of a TBC system. The samples are first heated in a furnace (Entech AB) at 1100 °C for 1 h and then cooled down for 10 min using compressed air to approximately 100 °C. These two steps are repeated until failure. The criterion for failure is deemed to be more than 20% visible spallation of the coating. A picture of the samples surface is taken at the end of each cycle using a webcam which is used later for calculating the number of cycles to failure.

3. Results

3.1 Image Analysis

Image analysis results for the substrate temperature sensitivity tests are presented in Fig. 3. As anticipated, the coating deposited at higher substrate temperature show lower porosity, although statistically not as significant. Figure 4 shows the microstructure taken using SEM for

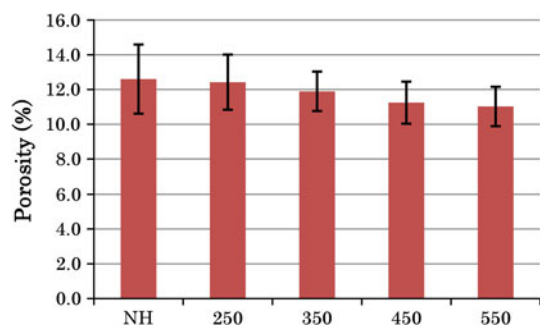


Fig. 3 Image analysis results from substrate temperature sensitivity tests, NH represents the coating with no external heating/cooling

the two extreme cases—no external heating/cooling and substrate temperature 550 °C. Any noteworthy differences between the microstructures were not observed with naked eye for these coatings for the spray parameter regime considered in this study. This could also be attributed to the fact that as the thermocouple measurements were made on the back side of substrate, the actual coating temperature might not be regulated during the experiment due to the presence of temperature gradient across the coating thickness. In addition, it is extremely difficult to statistically design an experiment where substrate temperature could be controlled independently without influencing other parameters. Due to these reasons, substrate temperature was not considered as a parameter for the DoE.

Coating thicknesses measured with optical microscopy are illustrated in Fig. 5. Coating thickness is an important parameter since it can affect TCF lifetime results. The target coating thickness was 500 μm as also highlighted in experiment number 3 (referred to as E3). As it can be observed, almost all coatings exhibited thickness close to the target thickness except for E6 coating. So the lifetime of E6 coating sprayed in this study might be lower than a coating sprayed with the target thickness (Ref 29).

Image analysis results for the DoE are presented in Fig. 6. The error bars represent one standard deviation. The center-point coatings in the DoE (E9, E10 and E11 in Fig. 2) show a typical porosity level for APS TBCs of around 10-12%. The high porosity level in low current and high spray distance coatings, that is, E3 and E7 can be clearly distinguished. This is somehow expected as lower current would imply lower energy particles during spraying, while higher spray distance would imply that particles have longer time to cool down which would again result in lower energy particles. As shown in earlier work (Ref 4), particles with lower energy result in higher porosity due to inferior filling of irregularities in the deposited splats. Moreover, higher powder feed rate would result in even lower energy particles during spraying, why E7 has the highest porosity level among all the sprayed coatings. However, the spray parameters for E7 coating would result in lower deposition efficiency which might be undesirable in production facilities.

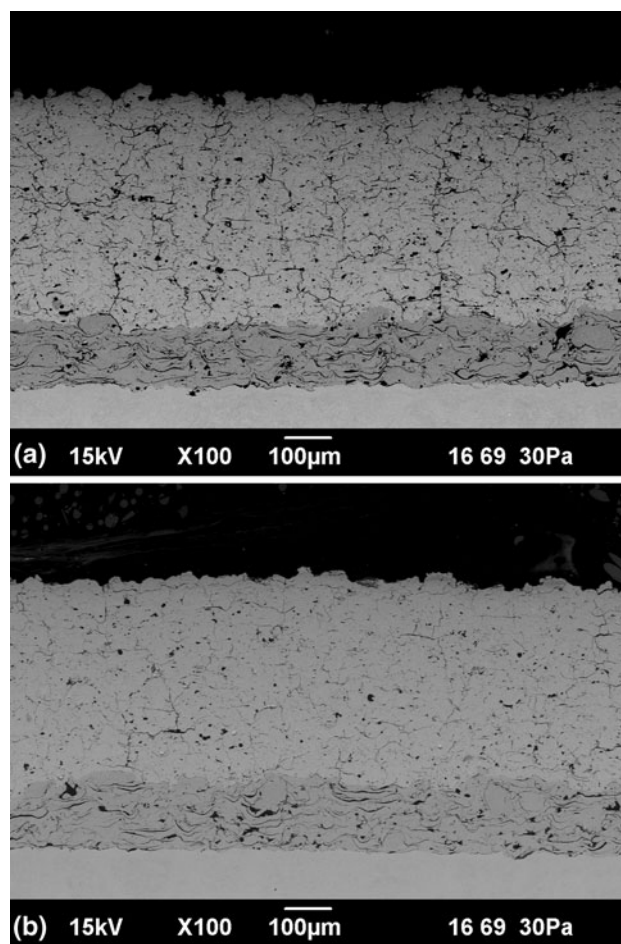


Fig. 4 Microstructure image taken using SEM from substrate temperature sensitivity tests for (a) no external heating/cooling and (b) substrate temperature 550 °C

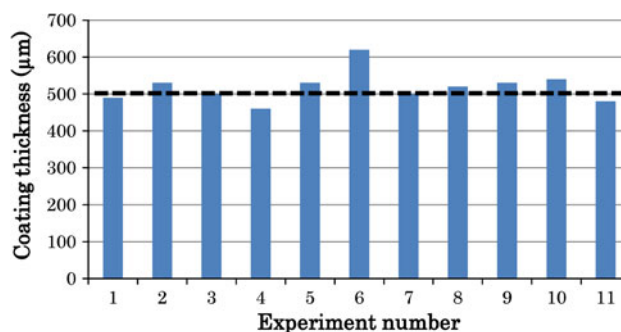


Fig. 5 Coating thickness measured using optical microscopy

3.2 Thermal Conductivity

Thermal conductivity results measured by laser flash technique are presented in Fig. 7, both for as-sprayed and heat-treated samples. Standard deviation for measurements in most cases ranged from 0.006 to 0.055 W/m·K, which is too small to be shown clearly on the data graphs, so it has been omitted. As expected, there is a significant rise in the thermal conductivity values after the heat

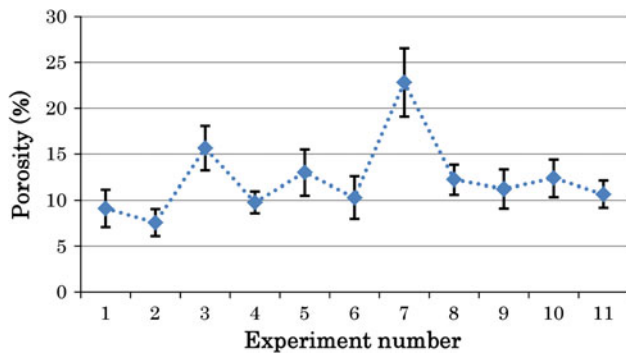


Fig. 6 Porosity level measurements

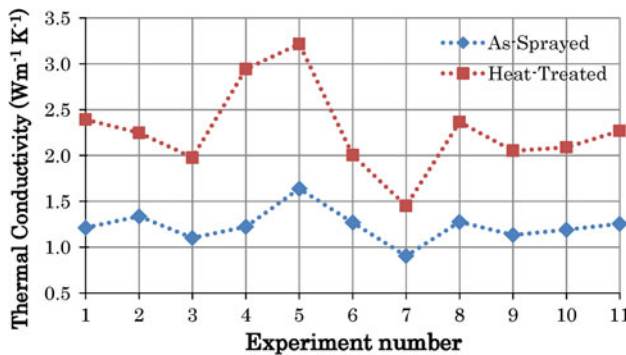


Fig. 7 Thermal conductivity results

treatment (Ref 30, 31). As can be seen in Fig. 7, E7 coating has the lowest thermal conductivity value. It also depicts the highest sintering resistance, as the thermal conductivity value shown raises the least for this coating after the heat treatment. E6 coating also shows comparable behavior to E7 coating. Other coatings, even though they have comparable values to E6 and E7 coatings in the as-sprayed state, show significantly lower sintering resistance. It must be noted here that the calculation of density from image analysis data can have significant impact on the thermal conductivity data. As an automated procedure was used for image analysis, same algorithm was used for analyzing all coatings. So if a coating exhibited large vertical cracks (for example E6, as discussed in section 4.1), the vertical cracks were also included in the calculated porosity which is typically not the case when reporting porosity level of coatings with large vertical cracks. This would result in an under-predicted value for thermal conductivity.

3.3 Young's Modulus and Nonlinear Degree

Young's modulus (E) and nonlinear degree (ND) results from ECP tests are presented in Fig. 8. The error bounds of these parameters are estimated at 3-5% of corresponding magnitudes based on earlier studies (Ref 17). E7 coating shows the lowest E value, while E3, E5, and E9 are other coatings with low E . Coatings with

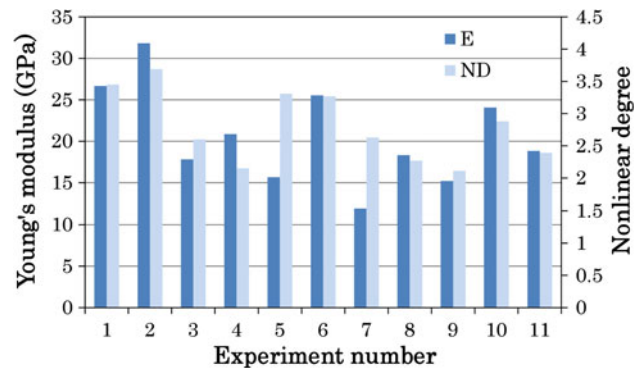


Fig. 8 ECP bi-layer curvature measurement results

high ND are E2, E5, and E6. Large variations can be observed among the sprayed set of coatings. It must be noted here that E and ND do not follow the similar trend for this set of coatings which means that a coating with low Young's modulus does not necessarily exhibit high non-linearity. The mechanical testing performance of these coatings will be discussed later in section 4.

3.4 Thermo-cyclic Fatigue Lifetime

TCF tests establish the capability of a coating system to survive long exposures at high temperature. Due to the size constraints of the platform in the furnace, the samples were run in two sets. Failure, in each case, seemed to be occurred due to the oxidation of the bondcoat because of cracks propagating through the topcoat-bondcoat interface. All the topcoats were completely spalled off at the end of the tests, with some having several cracks in them possibly due to induced thermal stresses and TGO growth.

TCF lifetime results are presented in Fig. 9. Some variations can be seen among the repeated center-point coatings in the DoE which demonstrates that there is a rather large natural variation. Despite this fact, it can be observed that E1, E5, E6, and E7 have significantly higher lifetime values than other coatings. E4 depicts exceptionally low lifetime, the reason for which will be discussed in next section. It must be remarked here that the lifetime in these tests is only influenced by mechanical compliance of the topcoats since the bondcoats are the same in all sprayed coatings.

3.5 Parameter-Property Statistical Correlations

The correlations between spray parameters and measured properties were plotted using the statistical software MODDE version 9.0 (MKS Umetrics AB, Sweden). Table 2 shows the influence of spray parameters on the properties along with the R^2 value which indicates the goodness of fit. Multiple linear regression (MLR) was chosen as the fit method for fitting the data. The confidence level for all plots was 95%. Parameters combinations other than the ones shown in Table 2 did not display a significant influence on the properties.

4. Discussion

4.1 Influence of Microstructure on Performance

As emphasized earlier, the effective mechanical and thermal properties are strongly dependent on the assembly of pores, cracks, and interfaces in sprayed coatings.

SEM microstructure images for E6, E7, and E10 coatings are presented in Fig. 10. E10, which is one of the centre points in the DoE, exhibits a typical APS TBC microstructure consisting of several globular pores and micro-cracks. E7 exhibits a highly porous microstructure with large globular pores evenly spread across the coating along with a few micro-cracks connected to the globular pores. On the contrary, E6 exhibits a dense microstructure with few globular pores but with several vertical and horizontal macrocracks, spread across the coating microstructure. As illustrated in section 3, both E6 and E7 showed the best performance, that is low thermal conductivity, high sintering resistance, and long lifetime. The high performance of similar microstructures has been noticed in earlier works too as discussed below.

The presence of long vertical cracks in microstructure, commonly referred to as segmentation cracks, has always been desired so as to replace the expensive electron beam—physical vapor deposition (EB-PVD) coatings in demanding applications. EB-PVD coating microstructures are highly strain tolerant with much longer lifetimes compared to APS coatings. Highly segmented TBCs with high-segmentation crack densities were obtained in the European ‘Toppcoat’ project (Ref 32). A common issue with this type of microstructures is that the vertical cracks lower the thermal resistance of the coating as they allow the flow of high temperature turbine gases, thus increasing

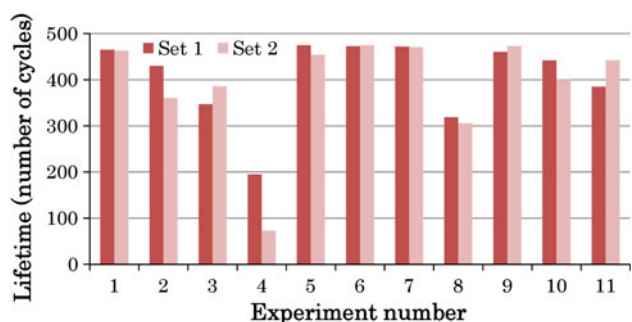


Fig. 9 TCF lifetime results—samples were run in two sets due to the size constraints of furnace platform

Table 2 Parameter-property statistical correlations

	R^2	CU	SD	PFR	CU × SD
Porosity ↑	0.932	↓	↑	↑	↓
Thermal conductivity ↑	0.673	↑
Young's modulus ↑	0.801	↑	↓	↓	...
Nonlinear degree ↑	0.686	...	↓
Lifetime ↑	0.856	↓	↓	↑	↓

‘...’ indicates that the parameter does not have a significant influence on the property. R^2 value indicates the degree of model fit. Thermal conductivity correlations were calculated for heat-treated samples. ↑ and ↓ indicates increase and decrease in values respectively

the heat transfer to the substrate (Ref 33). However, in the case of E6, as the vertical cracks do not penetrate throughout the coating, they do not affect the thermal conductivity value significantly. Moreover, the presence of horizontal macrocracks ensures that the thermal conductivity is low. Typically, horizontal cracks near the topcoat-bondcoat interface result in poor lifetime as they lead to early spallation of topcoat. However, in the case of E6 coating, the horizontal cracks are well distributed within the coating thickness (see Fig. 10b), thus resulting in an optimized microstructure with both low conductivity and long lifetime.

The influence of large globular pores in coating microstructure was observed in detail in an earlier work done by the same research group (Ref 30). In that work, a zirconia powder containing polymer as a porosity former was sprayed so as to artificially fabricate large globular pores by burning away the polymer after spraying. A similar microstructure as E7 was produced in this way. The samples were heat treated at 1150 °C for 100 h to study the effect of sintering on microstructure and thermal conductivity. It was found that the polymer porosity former coating performed the best compared to other coatings sprayed in that study, with lowest thermal conductivity and highest sintering resistance. In another recent work done by the authors, it was observed that polymer porosity former coating exhibits exceptionally high TCF lifetime (Ref 34). It was also shown that large globular pores with connected cracks inherited within the coating microstructure result in a coating with best performance. These results are consistent with the results of E7 coating fabricated in present study. The fabrication of E7 coating provides an alternative route for high performance coating microstructures rather than introducing artificial porosity by adding polymer to the YSZ powder.

4.2 Bi-layer Curvature Measurement Results

The evaluation of modulus provides indication of the coating integrity, porosity, and bonding quality between splats. It also provides an idea of the thermal stress developed in the coating during operation since the modulus is roughly proportional to the induced thermal stresses (Ref 27). ND essentially represents the change of stress-strain relation from its initial linear slope. In an earlier study, the ECP results were represented in the form of a E versus ND map and it was demonstrated that this approach can be linked to coating microstructure and its sensitivity to process condition (Ref 15).

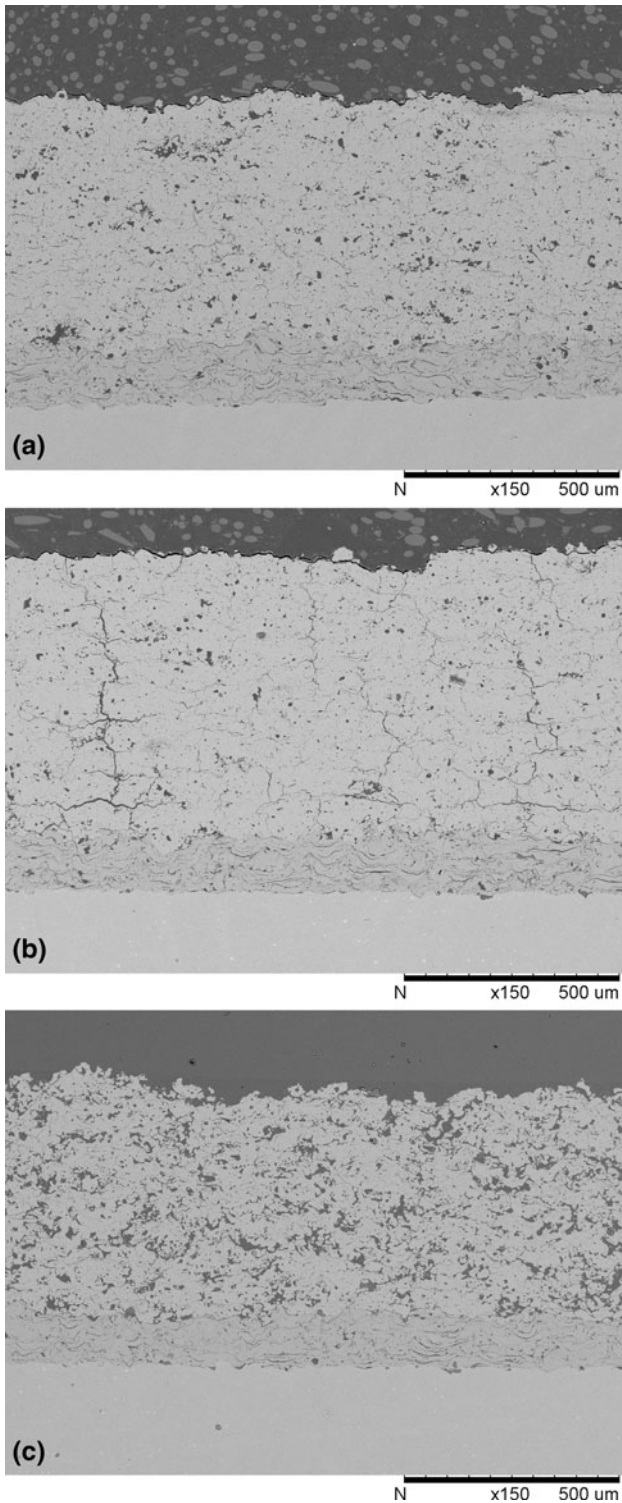


Fig. 10 Microstructure images for (a) E10, (b) E6, and (c) E7 coatings

In this study, the nonlinear parameters (ND and E) of the coatings were utilized to assess the repeatability of coatings as well as the coatings' nonlinear properties with changes in processing parameters. Figure 11(a) shows the

as-measured curvature and temperature data for coatings E9, E10, and E11. These coatings were sprayed at the beginning, middle, and end of the spraying session. E10 and E11 coatings show a good repeatability both in their curvature-temperature (κ - T) relationships as well as in microstructures. However, E9 coating exhibits significant difference in its anelastic behavior. Careful examination of microstructure revealed relatively higher porosity level associated with E9 coating. The microstructure images shown in Fig. 11(a) were taken from the coatings sprayed on ECP plates which revealed slight differences to the microstructure images taken from samples sprayed on square plates which included the bondcoat layer. The quantified nonlinear parameters for the three coatings shown in Fig. 11(b) support the observations made in Fig. 11(a). Coatings E10 and E11 occupy same location in E -ND map suggesting a good repeatability between the coatings. On the other hand, E9 coating falls at a lower elastic modulus region in the map supporting higher porosity observed in the coating as compared to E10 and E11 coatings. Origin of the differences in the coatings behavior in terms of nonlinear parameters are not very clear at this stage, however they can be, to a certain extent, attributed to the change in hardware or environmental conditions during deposition (Ref 3). Overall, Fig. 11 demonstrates the sensitivity of ECP measurements and nonlinear quantification of coatings even for subtle changes in coatings' architecture.

The effect of processing conditions on coatings' anelastic behavior is presented in Fig. 12. Figure 12(a) shows the κ - T plots for two coatings with significant differences in microstructures; E2 with significant high apparent vertical crack density and E7 with large population of globular and interlamellar pores. As shown in the figure, the E2 coating undergoes larger (approximately 50% more) curvature change as compared to E7 coating. Further, the E2 coatings showed significantly higher nonlinearity as compared to E7 coating which can be attributed to the higher crack density obtained by E2 coating. These visual differences are reflected in E -ND map shown in Fig. 12(b); E2 coating possesses higher E as well as ND as compared to E7 coating. Overall, Fig. 12(a) provides a perspective of a coating's κ - T relationship and its location in E -ND map.

Figure 12(b-d) shows a systematic shift in coatings nonlinear properties due to change in individual processing parameters considered for this study. The coatings with shorter spray distance (70 mm), E5, E1, E6, and E2, exhibit higher ND as well as E in the map as compared to those with longer spray distances (140 mm), E7, E3, E8, and E4, respectively. This shift can be attributed to the reduction of porosity (increasing elastic modulus) and increase in crack density (contributing to higher nonlinear degree) observed for the coatings sprayed at shorter spray distance.

Figure 12(c) provides the information about change in coatings nonlinear parameters with the change in spray gun current (CU). The coatings sprayed at higher current conditions (750 A) showed higher stiffness under ECP measurements than those deposited at lower current

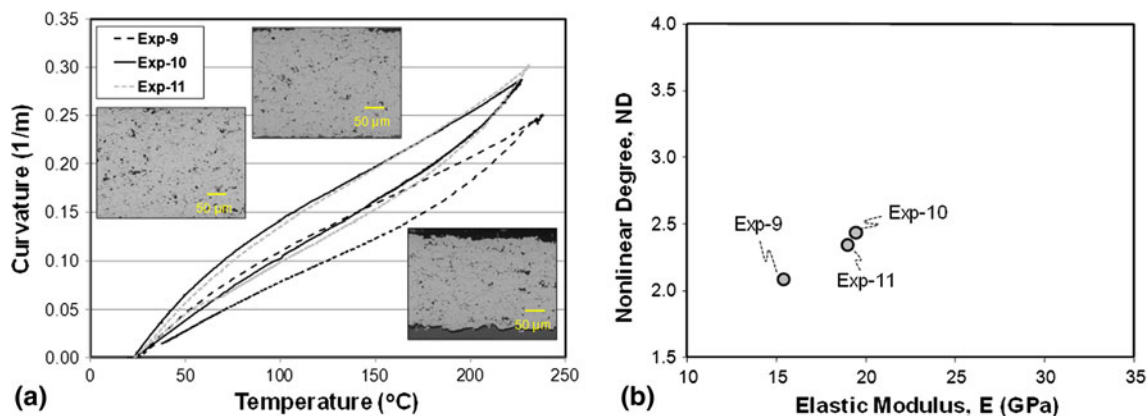


Fig. 11 ECP measurements for the coatings E9, E10, and E11: (a) curvature-temperature data and (b) anelastic parameters

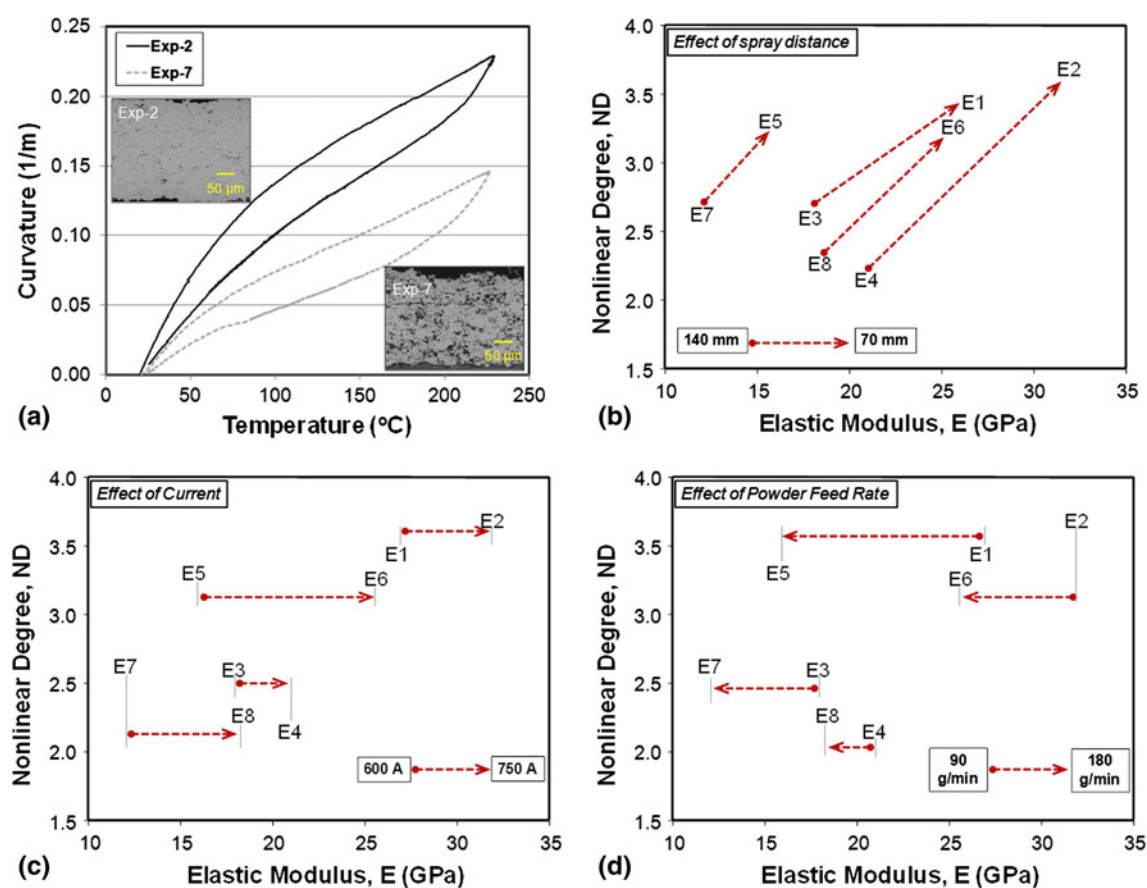


Fig. 12 Effect of processing conditions on ECP measurements (a) curvature-temperature data for E2 and E7 coatings, and effect of (b) spray distance, (c) current, and (d) powder feed rate, on anelastic parameters

conditions (600 A). It seems that the differences in net change in elastic modulus between a pair of low and high current conditions coatings depend on the pair. The largest difference is observed with E5 and E6 coatings, while for E3 and E4 coatings the change in elastic modulus was lowest.

Similar to Fig. 12(b) and (c), a systematic shift in coatings nonlinear property can be observed for changes

in the powder feed rate (90 versus 180 g/min). The results shown in Fig. 12(d) indicate that a reduction in coatings elastic modulus occurs with high powder feed rate. The net change in elastic modulus for a pair of coatings sprayed with low and high feed rate is different for each pair. The differences in ND values for the coatings with change in either current or powder feed rate do not exhibit a clear trend. Although, with the change in current, the

shift in ND values is larger with higher porosity coatings, which also possess lower ND values. In contrast, the difference in ND values is largest with denser or higher ND values coatings (E2 and E6) deposited with different powder feed rate. This could be attributed to different vertical crack characteristics in the two coatings.

Overall, the ECP measurements along with the E -ND map provide insights of coatings behavior which can be applied to establish detailed process-property correlations with microstructural insights. The high sensitivity of anelastic parameters can not only be utilized as an assessment of day-to-day coatings

4.3 Correlation Between ECP Bi-layer Curvature Results and TCF Lifetime

Assessing the lifetime of TBCs is a demanding task since testing them in real environments is very time consuming. TCF tests reduce the testing time significantly, but it could still require months to evaluate TCF lifetime. Even after being in use for more than three decades in gas turbine industry, TBCs are not fully integrated in the design due to lack of trustworthy lifetime database. Thus, reliable lifetime prediction by a swift alternate method is an important research target. A modeling approach has

been undertaken in several previous studies but the phenomena involved in TBC failure are far more complex to be efficiently captured by simulation (Ref 35, 36).

In the present study, with the help of microstructural observations, anelastic parameters and TCF lifetime results could be correlated as discussed below. Figure 13 shows the anelastic parameters of all coatings along with the microstructure images taken from the samples which included the bondcoat. The coatings are marked in three groups, differentiated according to their inherent microstructural features. Group A comprises the coatings which exhibited a dense microstructure with vertical cracks, group B contains the coatings which exhibited high porosity, and group C contains the rest of the coatings. The coatings with high lifetime (see Fig. 9) within the groups A and B in Fig. 13 have been marked out separately in different ellipses. It must be noted here that these groups were made according to the inherent microstructure details and do not directly reflect the coating properties.

In group A in Fig. 13, E1 and E6 coatings showed similar anelastic parameters- moderately high E and high ND, which resulted in high TCF lifetimes. However, E2 coating showed limited lifetime as compared to the E1 and E6 coatings. As it can be observed in Fig. 6, E2 coating has the lowest porosity value. This makes the coating

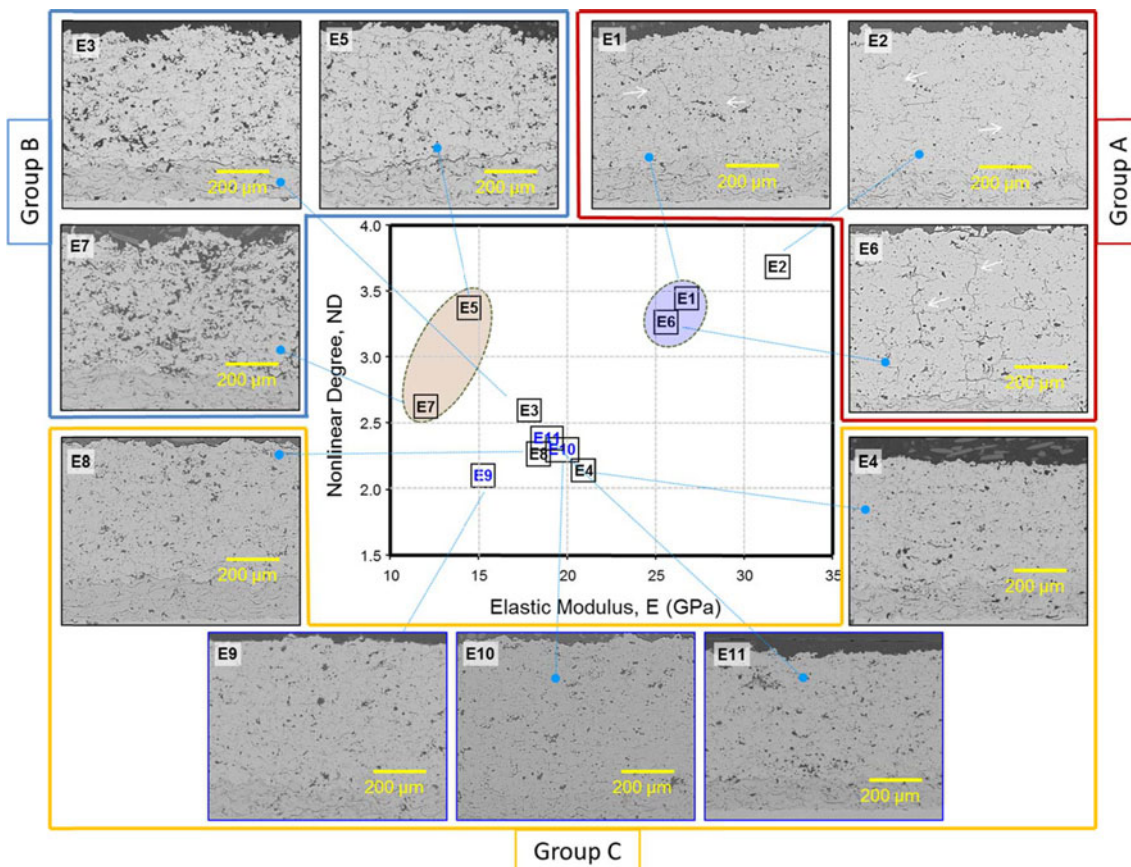
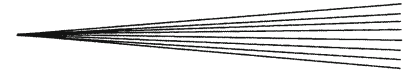


Fig. 13 Young's modulus vs. nonlinear degree map along with the coating microstructure images. The groups shown in the figure were made according to the inherent microstructure details and do not directly reflect the coating properties for the sprayed coatings



highly stiff with the highest Young's modulus among all the sprayed coatings, see Fig. 8. Thus, even if E2 coating has a high degree of nonlinearity, it showed highest elastic modulus among all indicating higher stiffness in coating, which might be the reason why it resulted in earlier failure in TCF tests than E1 and E6 coatings.

In group B in Fig. 13, E5 coating showed low E and high ND while E7 coating showed low E and moderately high ND. Both these porous coatings exhibited high lifetimes. On the other hand, E3 coating which showed moderately high E and ND showed earlier failure in TCF tests even though it exhibited high porosity.

All group C coatings showed moderately high E and low ND. All of these coatings exhibited low TCF lifetimes except E9 coating. A correlation between bi-layer curvature measurements and high TCF lifetime of E9 coating could not be found.

The observations above suggest that high nonlinear degree is beneficial to coating's TCF lifetime since all coatings with long lifetimes exhibited high ND. Moreover, it seems that there are two microstructure regimes for which this relationship holds—porous and vertically cracked, as marked by groups A and B in Fig. 13. For porous microstructure regime, coatings with low E and high ND exhibit long lifetime while for vertically cracked microstructure regime, coatings with high E and high ND also exhibit long lifetime, although there is a limit for the high value of E . This implies that the ECP results can be linked to the lifetime results with the help of a priori established microstructure analysis. It is believed that the reason for this correlation is that higher degree of nonlinearity will improve the strain tolerance of coatings which will result in better performance in lifetime tests.

The TCF test results could not be as significantly correlated with the anelastic parameters as compared to the relationships between process parameters and anelastic parameters. This could be due to the following reasons:

1. The substrates used for the bi-layer curvature measurement and TCF tests were of different materials and stiffness which might introduce variations in architecture of a coating on the two substrates. These variations could affect the coating property significantly.
2. Anelastic parameters are measure of coatings mechanical properties while TCF is a thermo-mechanical test, which is, unlike bi-layer curvature measurement, also controlled by thermal performance of coatings.
3. The anelastic parameters are obtained only for as-sprayed conditions for a coating, which does not incorporate well the changes in coating due to sintering. These parameters would be different for an aged coating; however, with the current stage of experimental set-up, it is not feasible to estimate them for a coating with sintering.

Despite the limitations stated above, these results illustrate that the bi-layer curvature measurements in

conjunction with appropriate microstructural analysis can be used as an indicator to predict the lifetime behavior of different APS TBCs. A major drawback with TCF lifetime tests is that they are very time consuming, which makes the combination of microstructural analysis and ECP sensor an attractive alternative as it does not require complex set-up or lengthy data interpretation.

5. Summary and Conclusions

An experimental approach was undertaken in this work to explore process microstructure-property relationships in TBCs with concomitant linkages to thermal cycle performance. A study evaluating the three crucial functional parameters in TBCs—thermal properties, mechanical properties, and lifetime, was performed and relationships between process parameters, microstructure and coating properties were established. Major conclusions from this study are as described below:

- Dense vertically cracked microstructure coating with low thermal conductivity and long lifetime was fabricated.
- An alternative route for fabricating high porosity microstructures with large globular pores and connected cracks inherited within the microstructure was provided. This type of microstructure exhibited the best performance in this study which was also in accordance with earlier work.
- A relationship between the nonlinear degree derived from beam curvature measurements and TCF lifetime based on a priori established microstructure analysis was proposed which may enable a predictive capability for coating response based on simplified experimental strategy. It was, however, observed that there are two microstructure regimes for which this relationship holds—porous and vertically cracked. The anelastic parameters need to be considered separately for these two regimes with further development of the interpretation.
- The results indicate that ECP bi-layer curvature measurements along with microstructure examinations can be used to optimize topcoat microstructures for TBC coatings. A more comprehensive study would be valuable to confirm the established relationships.

Acknowledgments

The authors would like to acknowledge The Knowledge Foundation for its financial support to the project and Volvo Aero Corporation for providing substrates and powders. The authors would like to thank Jimmy Johansson at Volvo Aero Corporation and Nicolaie Markocsan at University West for fruitful discussions and Stefan Björklund for his work on the spray experiments. The

international collaboration activity at Stony Brook University was supported in part by the NSF GOALI program under award CMMI 1030942.

References

1. N. Markocsan, P. Nylén, J. Wigren, and X.-H. Li, Low Thermal Conductivity Coatings for Gas Turbine Applications, *J. Therm. Spray Technol.*, 2007, **16**(4), p 498-505
2. A. Kulkarni, A. Vaidya, A. Goland, S. Sampath, and H. Herman, Processing Effects on Porosity-Property Correlations in Plasma Sprayed Yttria-Stabilized Zirconia Coatings, *Mater. Sci. Eng., A*, 2003, **359**(1-2), p 100-111
3. G. Dwivedi, T. Wentz, S. Sampath, and T. Nakamura, Assessing Process and Coating Reliability Through Monitoring of Process and Design Relevant Coating Properties, *J. Therm. Spray Technol.*, 2010, **19**(4), p 695-712
4. M. Friis, C. Persson, and J. Wigren, Influence of Particle In-Flight Characteristics on the Microstructure of Atmospheric Plasma Sprayed Yttria Stabilized ZrO₂, *Surf. Coat. Technol.*, 2001, **141**, p 115-127
5. M. Friis, "A Methodology to Control the Microstructure of Plasma Sprayed Coatings," Ph.D. Thesis, Lund University, 2002
6. A. Kucuk, C.G. Dambra, and C.C. Berndt, Influence of Plasma Spray Parameters on the Cracking Behavior of Yttria Stabilized Zirconia Coatings, *Pract. Fail. Anal.*, 2001, **1**(1), p 55-64
7. S.N. Basu, G. Ye, M. Gevelber, and D. Wroblewski, Microcrack Formation in Plasma Sprayed Thermal Barrier Coatings, *Int. J. Refract. Met. Hard Mater.*, 2005, **23**, p 335-343
8. G. Mauer, R. Vaßen, and D. Stöver, Atmospheric Plasma Spraying of Yttria-Stabilized Zirconia Coatings with Specific Porosity, *Surf. Coat. Technol.*, 2009, **204**, p 172-179
9. R. McPherson, The Relationship Between the Mechanism of Formation, Microstructure and Properties of Plasma-Sprayed Coatings, *Thin Solid Films*, 1981, **83**(3), p 297-310
10. Z. Wang, A. Kulkarni, S. Deshpande, T. Nakamura, and H. Herman, Effects of Pores and Interfaces on Effective Properties of Plasma Sprayed Zirconia Coatings, *Acta Mater.*, 2003, **51**(18), p 5319-5334
11. S. Sampath, Thermal Sprayed Ceramic Coatings: Fundamental Issues and Application Considerations, *Int. J. Mater. Prod. Technol.*, 2009, **35**(3-4), p 425-429
12. H.B. Guo, R. Vassen, and D. Stöver, Thermophysical Properties and Thermal Cycling Behavior of Plasma Sprayed Thick Thermal Barrier Coatings, *Surf. Coat. Technol.*, 2005, **192**(1), p 48-56
13. R. Vassen, F. Träeger, and D. Stöver, Correlation Between Spraying Conditions and Microcrack Density and Their Influence on Thermal Cycling Life of Thermal Barrier Coatings, *J. Therm. Spray Technol.*, 2004, **13**(3), p 396-404
14. T. Nakamura and Y.J. Liu, Determination of Nonlinear Properties of Thermal Sprayed Ceramic Coatings Via Inverse Analysis, *Int. J. Solids Struct.*, 2007, **44**(6), p 1990-2009
15. Y. Liu, T. Nakamura, V. Srinivasan, A. Vaidya, A. Gouldstone, and S. Sampath, Non-Linear Elastic Properties of Plasma-Sprayed Zirconia Coatings and Associated Relationships with Processing Conditions, *Acta Mater.*, 2007, **55**(14), p 4667-4678
16. Y.J. Liu, T. Nakamura, G. Dwivedi, A. Valarezo, and S. Sampath, Anelastic Behavior of Plasma-Sprayed Zirconia Coatings, *J. Am. Ceram. Soc.*, 2008, **91**(12), p 4036-4043
17. G. Dwivedi, T. Nakamura, and S. Sampath, Controlled Introduction of Anelasticity in Plasma-Sprayed Ceramics, *J. Am. Ceram. Soc.*, 2011, **94**(s1), p s104-s111
18. T. Wakui, J. Malzbender, and R.W. Steinbrech, Strain Analysis of Plasma Sprayed Thermal Barrier Coatings Under Mechanical Stress, *J. Therm. Spray Technol.*, 2004, **13**(3), p 390-395
19. T. Wakui, J. Malzbender, and R.W. Steinbrech, Strain Dependent Stiffness of Plasma Sprayed Thermal Barrier Coatings, *Surf. Coat. Technol.*, 2006, **200**, p 4995-5002
20. S.R. Choi, D. Zhu, and R.A. Miller, Mechanical Properties of Plasma-Sprayed ZrO₂-8 wt% Y₂O₃ Thermal Barrier Coatings, NASA/TM—2004-213216, 2004
21. S. Sampath, X.Y. Jiang, J. Matejcek, A.C. Leger, and A. Vardelle, Substrate Temperature Effects on Splat Formation, Microstructure Development and Properties of Plasma Sprayed Coatings. Part I: Case Study for Partially Stabilized Zirconia, *Mater. Sci. Eng., A*, 1999, **272**, p 181-188
22. J. Wigren, "High Insulation Thermal Barrier Systems—HITS", Brite Euram Project BE96-3226, 2002
23. R.E. Taylor, Thermal Conductivity Determinations of Thermal Barrier Coatings, *Mater. Sci. Eng., A*, 1998, **245**(2), p 160-167
24. J. Ilavsky, G.G. Long, A.J. Allen, and C.C. Berndt, Evolution of the Void Structure in Plasma-Sprayed YSZ Deposits During Heating, *Mater. Sci. Eng., A*, 1999, **272**, p 215-221
25. P. Strunz, G. Schumacher, R. Vassen, and A. Wiedenmann, In Situ SANS Study of Pore Microstructure in YSZ Thermal Barrier Coatings, *Acta Mater.*, 2004, **52**, p 3305-3312
26. Y. Tan, J.P. Longtin, S. Sampath, and H. Wang, Effect of the Starting Microstructure on the Thermal Properties of As-Sprayed and Thermally Exposed Plasma-Sprayed YSZ Coatings, *J. Am. Ceram. Soc.*, 2009, **92**(3), p 710-716
27. J. Matejcek and S. Sampath, In Situ Measurement of Residual Stresses and Elastic Moduli in Thermal Sprayed Coatings. Part I: Apparatus and Analysis, *Acta Mater.*, 2003, **51**, p 863-872
28. S. Sampath, V. Srinivasan, A. Valarezo, A. Vaidya, and T. Streibl, Sensing, Control, and In Situ Measurement of Coating Properties: An Integrated Approach Toward Establishing Process-Property Correlations, *J. Therm. Spray Technol.*, 2009, **18**(2), p 243-255
29. S. Stecura, Optimization of the NiCrAl-Y/ZrO₂-Y₂O₃ Thermal Barrier System, NASA-TM-86905, 1985
30. N. Curry, N. Markocsan, X.-H. Li, A. Tricoire, and M. Dorfman, Next Generation Thermal Barrier Coatings for the Gas Turbine Industry, *J. Therm. Spray Technol.*, 2011, **20**(1-2), p 108-115
31. N. Curry and J. Donoghue, Evolution of Thermal Conductivity of Dysprosia Stabilised Thermal Barrier Coating Systems During Heat Treatment, *Surf. Coat. Technol.*, 2012, **209**, p 38-43
32. R. Vassen, A. Stuke, and D. Stöver, Recent Developments in the Field of Thermal Barrier Coatings, *J. Therm. Spray Technol.*, 2009, **18**(2), p 181-186
33. I.O. Golosnoy, A. Cipitria, and T.W. Clyne, Heat Transfer Through Plasma-Sprayed Thermal Barrier Coatings in Gas Turbines: A Review of Recent work, *J. Therm. Spray Technol.*, 2009, **18**(5-6), p 809-821
34. M. Gupta, N. Curry, N. Markocsan, P. Nylén, and R. Vaßen, Design of Next Generation Thermal Barrier Coatings—Experiments and Modelling, *Surf. Coat. Technol.*, 2012, doi:10.1016/j.surfcoat.2012.09.015
35. D.M. Nissley, Thermal Barrier Coating Life Modeling in Aircraft Gas Turbine Engines, *J. Therm. Spray Technol.*, 1997, **6**(1), p 91-98
36. R. Vaßen, S. Giesen, and D. Stöver, Lifetime of Plasma-Sprayed Thermal Barrier Coatings: Comparison of Numerical and Experimental Results, *J. Therm. Spray Technol.*, 2009, **18**(5-6), p 835-845